Eur. Phys. J. D **42**, 273–278 (2007)
DOI: 10.1140/epjd/e2007-00037-5

THE EUROPEAN PHYSICAL JOURNAL D

Transition from bright to dark dissipative solitons in dielectric barrier gas-discharge

L. Stollenwerk[a], S.V. Gurevich, J.G. Laven, and H.-G. Purwins

Institut für Angewandte Physik, Corrensstraße 2/4, 48149 Münster, Germany

Received 19 July 2006 / Received in final form 21 December 2006
Published online 23 February 2007 –

Abstract. In this article we deal with the experimental investigation of pattern formation in a planar ac gas-discharge system with a dielectric barrier. We report on the first observation of the transition from bright to dark current filaments and vice versa via stripe-like patterns. The observed phenomena become classified in the framework of Turing-structures and solitary objects and are compared to results obtained by numerical simulations of a two-component reaction-diffusion-system.

PACS. 52.80.Hc Glow; corona – 89.75.Kd Patterns – 89.75.Fb Structures and organization in complex systems

1 Introduction

Self-organised patterns in nonlinear systems have been of increasing interest in recent years. Especially classical solitons and their non-conservative relatives, the dissipative solitons, turned out to be of particular interest for fundamental research as well as for application. Dissipative solitons have been found in very different areas of research. We only mention optical systems [1,2], semiconductor devices [3–6], electrical networks [7], nerve pulse transmission lines [8,9], chemical systems [10], and gas-discharge systems [11–13].

The present work concerns an ac-driven barrier discharge system (DBD) with a large aspect ratio which is known to produce a large amount of varying patterns, both particle-like structures [14–20] and other spatial patterns [21]. Usually, solitary filaments in such systems occur as current channels perpendicular to the dielectric barriers, defining a spot in the 2-dimensional discharge plane. These well localised objects and the corresponding well localised luminescence radiation density distribution we refer to as bright dissipative solitons. As a novelty, in the present experiments also dark solitons occur, consisting of a currentless, dark spot in an otherwise bright, homogeneous discharge. To obtain the transition between these two types of solitons only a single system parameter has to be varied. The intermediate states consist of different stripe-like patterns. Bifurcation scenarios like this are known from reaction-diffusion (RD) models [22,23], but to our knowledge experimental observations are rare [24]. A similar situation in a quasi one-dimensional electrical network was observed in [25].

[a] e-mail: stollenw@uni-muenster.de

In order to understand the above mentioned patterns and their transition scenario in the framework of pattern formation it is useful to clarify their relation to dissipative solitons on the one hand and to Turing structures on the other hand. As long as the pattern in question consists of well defined localised spots we want to refer to these objects as dissipative solitons. These dissipative solitons have a particle-like character and often exhibit interesting interaction phenomena. However, if there are many spots arranged in a spatially ordered way, usually in a hexagonal or quadratic lattice, from a phenomenological point of view they may be regarded as a Turing-like structure. Under a Turing pattern in this context we want to understand a static and spatially periodic pattern that emerges from a stationary homogeneous state by a bifurcation in which a well defined single wavelength becomes unstable. Thereby we assume that before and after the bifurcation the stationary state in a system with small extension is stable and the destabilisation of the spatially extended homogeneous state is due to diffusion.

To take the above considerations into account, the experimental results are discussed in the framework of a two-component reaction-diffusion equation. We numerically demonstrate an instability scenario, leading to high-amplitude patterns, which are similar to the experimental observations.

2 Experimental set-up

The experimental set-up is sketched in Figure 1. Both electrodes consist of glass plates coated with indium tin oxide (ITO), which is electroconductive and transparent with respect to the luminescence radiation being emitted from

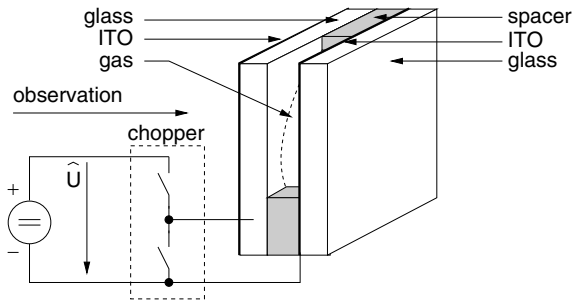

Fig. 1. Experimental set-up. Two glass plates of thickness a are separated by a spacer defining a circular gas-discharge space being filled with helium at pressure p and having the discharge length d and the diameter D. The glass plates both are coated with ITO, one of which is oriented to the gas space and the other to the outside. In the latter case the corresponding glass plate acts as a dielectric barrier. Through one of the glass plates the gas-discharge can be observed using a video camera. The system is driven by a positive rectangular voltage with a frequency f, a duty-cycle of 50% and an amplitude $\hat{U}$.

the gas during discharge. The latter being captured by appropriate cameras is to good approximation proportional to the current density. Between the glass plates there is a dielectric spacer defining a circular discharge area with diameter $D = 40$ mm and thickness $d = 0.5$ mm being the discharge length. One of the electrodes is oriented with the ITO coated side to the gas gap and therefore acts as a metallic electrode. At the other glass plate the ITO layer points to the outer side and hence acts as an electrode with a dielectric barrier with a thickness of $a = 0.5$–1.0 mm. Through one of the glass plates and the corresponding ITO layer the gas-discharge is observable by a video camera. The working gas in the gas gap is helium at a pressure of $p = 200$ hPa. The electric power supply provides a positive rectangular voltage with an amplitude up to $\hat{U} = 700$ V and a duty cycle of 50%. The frequency f is varied from 0.1 kHz to 20 kHz.

3 Experimental observations

The first run of the experiment was made by increasing the frequency. The experimental results are depicted in Figure 2. When the system is driven in the range of lower frequencies, a weak glow discharge with fluctuations in the light emission is visible. Figure 2 shows such a situation at $f = 6.2$ kHz. At higher frequencies the fluctuations increase, and at approximately 7.4 kHz bright spots occur arbitrarily distributed over the discharge area, as it is shown in Figure 2 for $f = 8$ kHz. Near the bifurcation point it is possible that spots are generated and disappear again. The three pictures in Figure 2 at $f = 8$ kHz represent such a scenario. They are taken from consecutive video frames with a repetition time of 20 ms. In the first frame the upper of three bright spots has just been ignited. In the second frame it is fully developed and in the third frame it has vanished again. As the frequency is further increased more and more spots arise. At

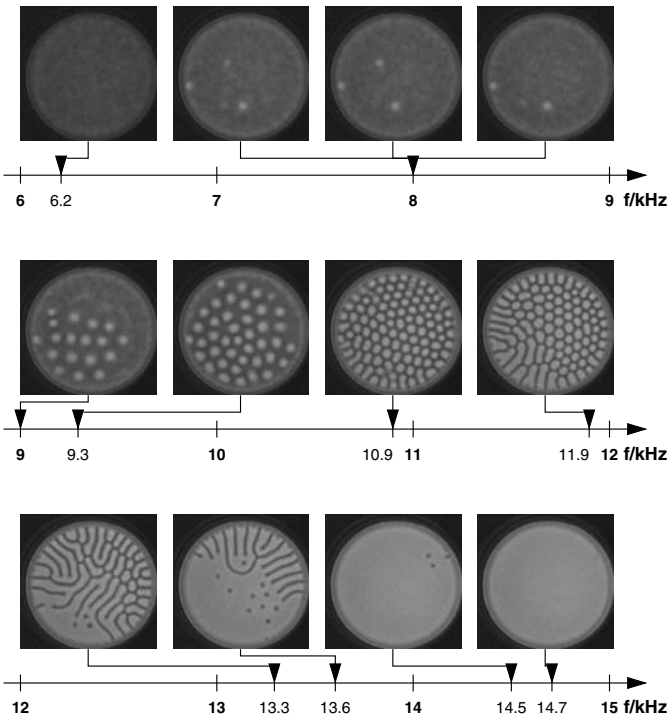

Fig. 2. Luminescence radiation density being emitted from the DBD system as the driving frequency f is increased. The three pictures at $f = 8$ kHz are consecutive video frames with a repetition time of 20 ms. The parameters according to Figure 1 are $a = 0.7$ mm, $d = 0.5$ mm, $D = 40$ mm, $p = 200$ hPa He, $U = 550$ V, exposure time: 1/250 s.

$f = 9$ kHz almost half of the discharge area is covered with spots. From time to time some rearrangement of the pattern occurs which becomes increasingly vivid with further increase of the frequency. At $f = 9.3$ kHz the whole discharge area is covered with bright spots. Due to the large number of spots they are rather near to each other and spots formally having radial symmetry become deformed due to interaction. In Figure 2 at $f = 10.9$ kHz a dense arrangement of deformed spots is shown. For $f \gtrsim 9.3$ kHz the pattern undergoes continuous rearrangement.

When the frequency is increased further, the spots begin to fuse with their neighbours as it is shown in Figure 2 at $f = 11.9$ kHz. Hence for these objects it is no longer evident that they are spots on a dark background. In fact, it seems to be more justified to refer to a bright background with areas of lower light intensity. For further increase of the frequency the pattern consists of a bright background with dark, branched grooves, as it is shown in Figure 2 at $f = 13.3$ kHz. At this point it becomes evident that the dark stripes always hit the boundary of the discharge area at right angle. Eventually some grooves become very short, and if they are as short as they are broad one would prefer to refer to them as spots. When the frequency is still increased further we occasionally observe dark spots (Fig. 2 at $f = 13.6$ kHz) performing an irregular shivering and propagation. At $f = 14.5$ kHz the discharge plane exhibits an almost homogeneous bright luminescence radiation background and only a few dark spots are left.

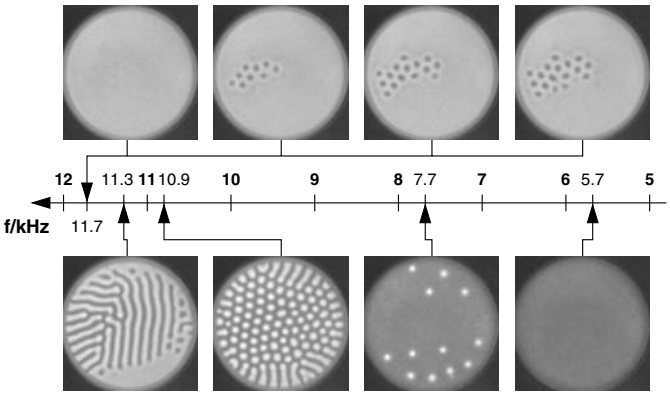

Fig. 3. Luminescence radiation density emitted from the DBD system as the driving frequency f is decreased. The four pictures at $f = 11.7$ kHz are consecutive video frames with a repetition time of 20 ms. The parameters and exposure time are as in Figure 2.

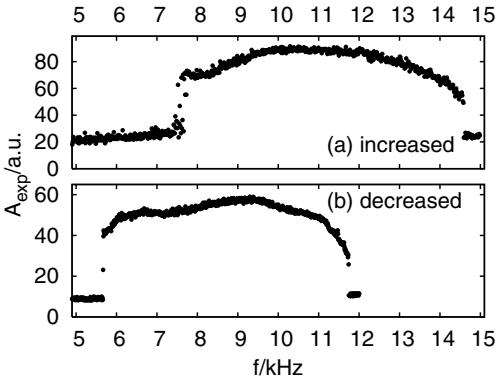

Fig. 4. Amplitude difference A_{exp} of the pattern in dependence of the driving frequency: (a) for increasing frequency, evaluated from Figure 2; (b) for decreasing frequency, evaluated from Figure 3.

Finally, at $f = 14.7$ kHz all dark spots have disappeared and a homogeneous glow discharge covers the whole discharge area. This state stays stable up to the driving frequency of 20 kHz.

In a subsequent experiment the driving frequency has been decreased. The emerging patterns are presented in Figure 3. In the beginning, the discharge exhibits a nearly homogeneous bright glow. At $f = 11.7$ kHz the first dark spots arise. Their appearance is shown in Figure 3 in the upper row in four subsequent frames. The leftmost image belongs to the highest frequency. In contrast to the bright spots in the first run, the dark spot arise close to each other forming a connected island that grows with decreasing driving frequency. As the driving frequency becomes even smaller, the same patterns as in the first run occur in the reverse order (Fig. 3, upper row). Finally, at about $f = 5.7$ kHz, the last bright spot disappears.

In Figure 4 the amplitude difference A_{exp} of the pattern in dependence of the driving frequency is depicted. We define this amplitude difference A_{exp} as the difference of luminescence intensities between the brightest and the darkest area in the pattern. To reduce the influence of noise, the local brightness in a camera frame is computed as the average over a small area. The size of that area is chosen to be much smaller than the lateral structures in the pattern and large enough to reduce the noise sufficiently. To avoid effects of the boundary only the inner circle with a diameter of 32 mm of the discharge area is considered.

In Figure 4a below approximately $f = 8$ kHz the amplitude is determined only by the noise in the slightly glowing discharge. At approximately $f = 8$ kHz the first bright filaments occur and the amplitude jumps to a higher value. Within the jump some frames with intermediate amplitude occur. This is due to switching on and off of filaments during the exposure time. With increasing driving frequency the pattern varies from bright spots over stripes to dark spots and, the pattern amplitude develops continuously. At approximately $f = 14.5$ kHz, when the last dark spot disappears, the amplitude falls back to the low level of a homogeneous discharge.

In Figure 4b the amplitude difference A_{exp} corresponding to Figure 3 is to be seen. The onset of the pattern at $f = 11.7$ kHz occurs abruptly. In the course of further increase of f the experiment the amplitude difference A_{exp} develops continuously. At $f = 5.7$ kHz the pattern has disappeared and A_{exp} falls back to the noise level. There is a single frame with an intermediate amplitude of 23 a.u. corresponding to a switching filament.

As inferred from Figure 4 bifurcations from the homogeneous state to the patterned state are subcritical, and one might expect a hysteresis in the bifurcation point depending on the direction of the change of f. Although the overall phenomenon is reproducible, the precise positions of the discontinuities vary from run to run over a wide range, i.e. from 4 to 8 kHz and from 9 to more than 20 kHz for the lower and upper transitions respectively. Therefore so far it is impossible to investigate the hysteresis of the reported bifurcations in detail.

4 Comparison with results of a reaction-diffusion system

There are two classical approaches to describe the plasma in the gas discharge, namely particle based models (e.g. PIC) [26] and fluid based modes (i.e. drift-diffusion [27]) and many variations and combinations of them. The first approach is very basic, and valid for a wide range of plasma parameters, but generally covers a time span of less than 1 μs. For the latter one this range goes up to several tens of micro-seconds. The dynamics in our system take place on a time scale of 0.1–1 s, so numerical simulations for both cases are not practicable, at least with presently available computers. Since on the other hand reliable analytical solutions of the transport equations seem to be far from reachable we conclude that a straight forward interpretation of the experiment seems to be inaccessible on the basis of present theoretical knowledge of gas discharge.

To be still able to classify the observed patterns and understand the bifurcations in between, we will follow a

synergetic approach and use a simple model with qualitatively similar solution behaviour, namely a reaction-diffusion (RD) system. The most obvious hint that this approach is promising is given by the similarity of the patterns and instability scenarios seen in the experiment and those observed in RD systems [22–24,28,29]. This assumption is further supported by the fact that for a DC-system in a similar parameter range and similar large aspect ratio the lateral structuring is proved to be described by a lateral RD model [30–32]. For the DBD system we investigate in this work, the association of RD model quantities with physical quantities is topic of actual research. First hints for the link between the viewpoints of gas discharge physics and RD concepts are given in the discussion of this article.

RD systems usually exhibit very general behaviour, so that even models without a specific connection to the actual experimental system can describe emerging patterns qualitatively very well and explain the types of observed bifurcations. In this sense, similar patterns have been studied in different chemical [23,28], physical [29] and biological [22,24] systems. Also gas-discharge systems have been successfully described qualitatively with reaction-diffusion models [33–35]. The aim of a RD model describing a physical system is not to give the best possible quantitative prediction but to classify the observed patterns and bifurcations. Keeping that in mind, we choose a simple two-component RD system with only one nonlinearity:

$$\begin{aligned} \partial_t u &= D_u \Delta u + \lambda u - u^3 - v + \kappa_1 - \kappa_2 \langle u \rangle, \\ \tau \partial_t v &= D_v \Delta v + u - v, \end{aligned} \tag{1}$$

where $u = u(r,t)$ and $v = v(r,t)$, $r \in \Omega \subset \mathbb{R}^2$. The parameters D_u, D_v, τ, λ and κ_2 are positive, whereas the sign of κ_1 is arbitrary. The term $\langle u \rangle$ denotes the spatial average, describing a global feedback effect, namely

$$\langle u \rangle = \frac{1}{|\Omega|} \int_\Omega u(r,t) dr.$$

This system can be considered as an extension of the FitzHugh-Nagumo equation for nerve pulse transmission [8,9], which is widely used to model some biological [36], chemical [37] and physical systems [13,38]. For appropriate parameters u in system (1) can be considered as an activator stimulating the temporal evolution of the two variables u and v while v acts as an inhibitor. The only nonlinearity comes into play through the cubic term in the first equation. The system parameters were chosen in such a way, that equations (1) admit only one homogeneous solution, which is stable in a certain parameter region. Notice that this solution can become unstable with respect to finite wave number perturbation (Turing instability) if one changes some control parameter.

A distinct feature of the system (1) is the presence of the integral term $\langle u \rangle$. In this case, the well-known conditions of Turing instability (see, e.g., [3,34,39]) are not affected, but the homogeneous solution is shifted. If one chooses κ_1 as a control parameter, the critical value for the onset of the Turing instability is

$$\kappa_{1c} = \pm \sqrt{\frac{\lambda - \sigma}{3}} \left(1 + \kappa_2 - \frac{2\lambda + \sigma}{3} \right), \tag{2}$$

where $\sigma = 2\sqrt{D_u/D_v} - D_u/D_v$.

We study this model by solving the system (1) numerically with zero flux boundary conditions on a rectangular domain $\Omega = [0,5] \times [0,5]$. In the beginning, the value of κ_1 is set to 1.72 and the initial condition is the random perturbed uniform solution. When the simulation reaches a stationary state, a further simulation is started with decreased κ_1 and with the previous stationary state as the initial condition. In this way, we calculate the emerging patterns for all $\kappa_1 \in [-\kappa_{1c}, \kappa_{1c}]$. In Figure 5 an example from this series of calculations is to be seen.

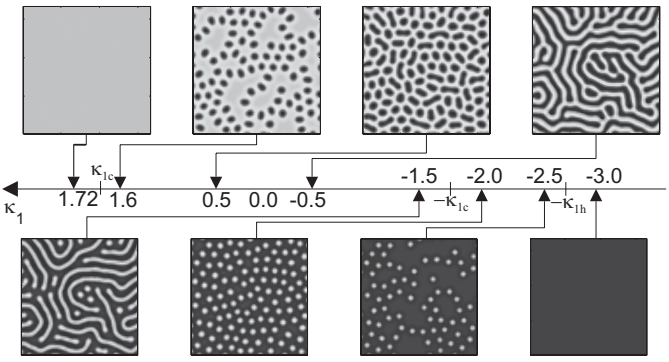

Fig. 5. Typical stationary solutions of system (1) if the control parameter κ_1 is decreased. Parameters: $D_u = 2.8 \times 10^{-4}$, $D_v = 5.0 \times 10^{-3}$, $\lambda = 0.9$, $\kappa_2 = 4.0$, $\tau = 1.0$, $\kappa_1 \in [-3.0, 3.0]$. The critical values are $\kappa_{1c} = \pm 1.709$. Boundary conditions are Neumann.

Below the threshold $\kappa_{1c} = 1.709$ the uniform state becomes unstable in favour of a finite wave number perturbation. The emerging spot-like pattern is shown in Figure 5 for $\kappa_1 = 1.6$. The spots consist of low u areas (dark) on a high u (bright) background. Notice, that as the system is in a subcritical regime (forcing a high-amplitude pattern) and because of the presence of the integral term (limiting the overall activator density), the pattern is not periodic in space, but only some wave trains emerge. In the course of further decrease of κ_1 the pattern significantly changes its shape: spot-like pattern (see Fig. 5, $\kappa_1 = 0.5$), labyrinths ($\kappa_1 = -0.5$), and labyrinth patterns with bright spots ($\kappa_1 = -1.5$). Finally, one observes spot-like patterns with high u (bright) spots on a low u (dark) background ($\kappa_1 = -2.0$, $\kappa_1 = -2.5$). In contrast to the previously seen, Turing triggered patterns, these spots do not form coherent wave trains. The number of spots decreases for decreasing values of κ_1. When κ_1 falls below -2.72, the pattern vanishes and the homogeneous solution emerges (see Fig. 5, $\kappa_1 = -3.0$). This second critical value of κ_1, being different from $-\kappa_{1c}$, we refer to as $-\kappa_{1h}$.

A similar numerical simulation was made with increasing κ_1, starting from $\kappa_1 = -2.72$. As equations (1) are symmetric with respect to a change of sign, the emerging

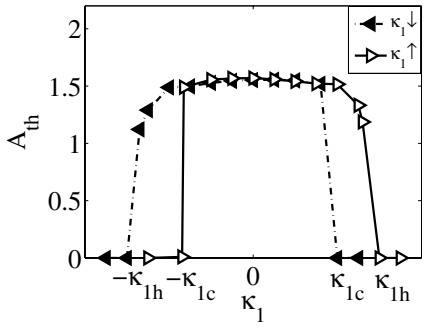

Fig. 6. Dependence of the activator amplitude $A_{\rm th}$ on the control parameter for increased (△) and decreased (▲) values of κ_1. Parameters are the same as in Figure 6.

patterns are qualitatively the same as in Figure 5 with exchanged bright (high u) and dark (low u) areas. The onset of the Turing instability then occurs at $-\kappa_{1c} = -1.709$, and at $\kappa_{1h} = 2.72$ the pattern vanishes.

To investigate the type of the observed bifurcations, we calculate from the results gained numerically the pattern amplitude difference $A_{\rm th}$ of the activator u as a function of κ_1. $A_{\rm th}$ is defined as the difference between the largest and the smallest value of u within Ω. Due to the used numerical accuracy a noise rejection for u is not necessary. The result is shown in Figure 6 for decreasing (solid triangles) and increasing (open triangles) κ_1.

On this background the behaviour of the system can be understood as follows: for $|\kappa_1| > \kappa_{1h}$ the system (1) is in a homogeneous stable state, corresponding to the zero amplitude $A_{\rm th}$. For $|\kappa_1| < \kappa_{1c}$ the system is in a patterned state. The amplitudes $A_{\rm th}$ for all parameter values in this region are almost the same. The bifurcations taking place if $|\kappa_1|$ crosses κ_{1c} or κ_{1h} are subcritical. For $|\kappa_1| \in [\kappa_{1c}, \kappa_{1h}]$ there are hysteresis regions, i.e. the actual value of the amplitude $A_{\rm th}$ is determined by the initial condition of the calculation, i.e. the direction of κ_1 variation. The patterns in these regions consist of solitary spots being not connected to each other (see Fig. 5).

5 Discussion

In the experimental part of this work we presented a DBD system exhibiting both bright current spots in a low current, dark surrounding and low current, dark spots within an otherwise homogeneously high current surrounding. The transition between these patterns is mediated by stripe-like patterns. We now want to classify these phenomena in the framework of dissipative solitons and Turing structures.

To begin with, spots behaving like dissipative solitons shall be identified. In both measurements, Figure 2 (increasing driving frequency) and Figure 3 (decreasing driving frequency), they appear at the end of the recording shortly before the pattern vanishes in favour of a homogeneous system state. For increasing driving frequency (Fig. 2) examples can be found in the images at $f = 13.6$ kHz and $f = 14.5$ kHz. For decreasing driving frequency (Fig. 3) they are exemplarily shown at $f = 7.7$ kHz. They can be identified as dissipative solitons by means of their arbitrary distances (i.e. their lack of long distance order) and their independent movement.

There are also a couple of spots in the beginning of both recordings, when the homogeneous state becomes unstable in favour of a structured discharge. For decreasing driving frequency (Fig. 3, $f = 11.7$ kHz) these spots appear as a domain of agglomeration with distinct short range order. As the driving frequency decreases, the domain of spots grows but spots existing independently do not appear. In combination with the amplitude behaviour (Fig. 4b) indicating a subcritical bifurcation, this pattern can safely be identified as a subcritical Turing bifurcation limited by a globally acting inhibition. For increasing driving frequency (Fig. 2) the situation is more complicated. For low frequencies ($f = 8$ kHz) single bright spots with arbitrary distances appear. But in contrast to the dark spots at the end of this recording and also in contrast to the bright spots at the end of the recording with decreasing driving frequency (Fig. 3, $f = 7.7$ kHz), these spots do not move at all. Moreover, they appear at rather low frequencies (at $f = 8$ kHz), long before the discharge area becomes covered with further spots (at $f = 9$ kHz). This leads us to the conclusion, that these early bright spots are induced by inhomogeneities or defects on the dielectric surfaces and are not truly self-organised. The following occupation of the discharge area with further bright spots (Fig. 2, $f = 9$ kHz) as the driving frequency increases is very similar to the appearance of dark spots with decreasing driving frequency (Fig. 3, $f = 11.7$ kHz – $f = 9.3$ kHz). The filaments occur in an agglomerated manner with a rather well defined short range order. Again, with respect to the behaviour of the amplitude $A_{\rm exp}$ (Fig. 4a) indicating a subcritical bifurcation, this bifurcation can be classified as a Turing bifurcation limited by a globally acting inhibition. Also in the present experimental situation, the physical nature of the global inhibition might be some serial resistance, i.e. the internal resistance of the driving.

Finally, we want to compare the experimental findings to the results obtained from the RD-model. As the model is not specific for our gas-discharge system, we cannot draw any quantitative comparisons. However, a qualitative comparison is possible.

First, consider the development of the amplitude $A_{\rm exp}$ of the patterns as they are shown in Figure 4 for the experiment and as $A_{\rm th}$ in Figure 6 for the RD-model. In both cases, all bifurcations — from a homogeneous state to a structured one and vice versa — are subcritical. In the course of the high-amplitude patterns the amplitude changes continuously.

For the pattern amplitude behaviour $A_{\rm th}$ in the model (Fig. 6) the region of hysteresis of the subcritical bifurcations can be identified in the intervals $[\kappa_{1c}, \kappa_0]$ and $[-\kappa_0, -\kappa_{1c}]$ respectively. In the experiment, the range and the position of the high-amplitude patterns varies over a wide area between single runs making it impossible to compare the bifurcation points obtained from different runs. Nevertheless, as argued above, a region of hysteresis cannot be determined though is very probable.

Furthermore the comparison of the observed patterns in the experiment (Figs. 2 and 3) and the RD-model (Fig. 5) leads to remarkable agreement. The appearance of spots, bright ones as well as dark ones, occurs via a subcritical Turing bifurcation limited by integral inhibition. The intermediate patterns in both cases consist of branched stripe-like patterns with a spatial scale inherited from the spots.

We found the patterns in the luminescence radiation density in the experiment and in u in the RD-model to be similar, therefore the model quantity u is supposed to be related to the current density j (which is known to be proportional to the luminescence density [20,40]) in the experiment. Also the surface charges an the dielectric barriers contribute to the activatory effect of u at the beginning of each breakdown. The inhibitory effect of the model variable v is related to volume and surface charges within each breakdown. A detailed discussion of the mentioned physical quantities is given in [41].

We want to thank Dr. Sh. Amiranashvili for fruitful discussions and for reading the manuscript. We thank the Deutsche Forschungsgemeinschaft (DFG) for financial support.

References

1. T. Ackemann, W. Lange, Appl. Phys. B **72**, 21 (2001)
2. N. Akhmediev, A. Ankiewicz, *Dissipative Solitons*, Lecture Notes in Physics (Springer, Berlin, 2005)
3. F.-J. Niedernostheide, M. Arps, R. Dohmen, H. Willebrand, H.-G. Purwins, Phys. Stat. Sol. (b) **172**, 249 (1992)
4. E. Schöll, F.J. Niedernostheide, J. Parisi, W. Prettl, H.-G. Purwins, *Formation of spatio-temporal structures in semiconductors,* edited by F.H. Busse, S.C. Müller, pages 446–494, 1998
5. E. Schoell, *Nonlinear Spatio-Temporal Dynamics and Chaos in Semiconductors*, volume 10 of Cambridge Nonlinear Science Series (Cambridge University Press, Cambridge, 2001)
6. K. Aoki, *Nonlinear Dynamics and Chaos in Semiconductors* (Institute of Physics Publishing, Bristol and Philadelphia, 2001)
7. T. Dirksmeyer, R. Schmeling, J. Berkemeier, H.-G. Purwins, *Experiments on the formation of stationary spatial structures on a network of coupled electrical oscillators,* edited by D. Walgraef, N.M. Ghoniem Patterns, Defects and Materials Instabilities, pages 91–107 (Nato ASI Series E: Applied Sciences, 1990)
8. R. FitzHugh, Biophys. J. **1**, 445 (1962)
9. J. Nagumo, S. Arimoto, S. Yoshizawa, Proc. Inst. Radio Engineer. Electron **50**, 2061 (1962)
10. K.-J. Lee, W.D. McCormick, J.E. Pearson, H.L. Swinney, Nature **369**, 215 (1994)
11. H. Willebrand, C. Radehaus, F.-J. Niedernostheide, R. Dohmen, H.-G. Purwins, Phys. Lett. A **149**, 131 (1990)
12. E. Ammelt, D. Schweng, H.-G. Purwins, Phys. Lett. A **179**, 348 (1993)
13. H.-G. Purwins, H.U. Bödeker, A.W. Liehr, *Dissipative solitons in reaction-diffusion systems,* edited by N. Akhmediev, A. Ankiewicz, Dissipative Solitons (Springer, Berlin Heidelberg, 2005)
14. L.F. Dong, X.C. Li, Z.Q. Yin, S.F. Qian, J.T. Ouyang, L. Wang, Chin. Phys. Lett. **18**, 1380 (2001)
15. L. Dong, Z. Yin, L. Wang, G. Fu, Y. He, Z. Chai, X. Li. Thin Solid Films **435**, 120 (2003)
16. I. Müller, E. Ammelt, H.-G. Purwins, Interaction of filaments in a A.C.-driven planar gas discharge system, In *Int. Conf. on Phenoma in Ionized Gases ICPIG XXIII*, volume II-182 - II-183, Toulouse, France, 17.7.-22.7.1997, 1997
17. I. Müller, E. Ammelt, H.-G. Purwins, Phys. Rev. Lett. **82**, 3428 (1999)
18. I. Brauer, E. Ammelt, H.-G. Purwins, Double breakdowns in a pattern forming dielectric barrier discharge system, In *Proc. XXIV Intern. Conf. on Phenomena in Ionized Gases (ICPIG)*, pages 141–142, July 11-16, 1999, Warschau, 1999
19. L. Stollenwerk, Sh. Amiranashvili, J.-P. Boeuf, H.-G. Purwins, Phys. Rev. Lett. **96**, 255001 (2006)
20. I. Brauer, Experimentelle und numerische Untersuchungen zur Strukturbildung in dielektrischen Barrierenentladungen, Ph.D. thesis, Westfälische Wilhelms–Universität Münster (2000)
21. E.L. Gurevich, A.L. Zanin, A.S. Moskalenko, H.-G. Purwins, Phys. Rev. Lett. **91**, 154501-1 (2003)
22. E. Meron, E. Gilad, J. von Hardenberg, M. Shachak, Y. Zarmi, Chaos Solitons Fractals **19**, 367 (2004)
23. B. Peña, C. Pérez-García, Phys. Rev. E **64**, 056213 (2001)
24. J. von Hardenberg, E. Meron, M. Shachak, Y. Zarmi, Phys. Rev. Lett. **87**, 198101 (2001)
25. H.-G. Purwins, C. Radehaus, *Pattern formation on analogue parallel networks,* edited by H. Haken, "Neural and Synergetic Computers" (Springer Series in Synergetics, 1988), Vol. 42, pp. 137–154
26. R.W. Hockney, J.W. Eastwood, *Computer simulation using particles* (IOP Publishing, 1988)
27. J.P. Boeuf, J. Phys. D **36**, R53 (2003)
28. P. Borckmans, A. De Wit, G. Dewel, Physica A **188**, 137 (1992)
29. W. Just, M. Bose, S. Bose, H. Engel, E. Schöll, Phys. Rev. E **64**, 026219 (2001)
30. M.S. Benilov, Phys. Rev. A **45**, 5901 (1992)
31. R. Sh. Islamov, Phys. Rev. E **64**, 1 (2001)
32. Sh. Amiranashvili, S.V. Gurevich, H.-G. Purwins, Phys. Rev. E **71**, 066404 (2005)
33. H.-G. Purwins, C. Radehaus, T. Dirksmeyer, R. Dohmen, R. Schmeling, H. Willebrand, Phys. Lett. A **136**, 480 (1989)
34. C. Radehaus, H. Willebrand, R. Dohmen, F.-J. Niedernostheide, G. Bengel, H.-G. Purwins, Phys. Rev. A **45**, 2546 (1992)
35. M. Bode, H.-G. Purwins, Physica D **86**, 53 (1995)
36. J.D. Murray, *Mathematical Biology* (Springer, Berlin, 1993)
37. *Chemical Waves and Patterns*, edited by R. Kapral, K. Showalter, "Understanding Chemical Reactivity" (Kluwer Academic Publishers, Dordrecht, 1995), Vol. 10
38. H. Engel, F.-J. Niedernostheide, H.-G. Purwins, E. Schöll, *Self-Organization in Activator-Inhibitor-Systems: Semiconductors, Gas-Discharge and Chemical Active Media.* (Wissenschaft und Technik Verlag, Berlin, 1996)
39. R. Kapral, Physica D **86**, 149 (1995)
40. L. Stollenwerk, J.G. Laven, H.-G. Purwins, Phys. Rev. Lett. (submitted)
41. L. Stollenwerk, Sh. Amiranashvili, J.-P. Boeuf, H.-G. Purwins, Eu. Phys. J. D (submitted)